https://doi.org/10.2352/ISSN.2470-1173.2020.15.COLOR-123

Colorimetrical performance estimation of a reference hyperspectral microscope for color tissue slide assessment

Paul Lemaillet, Wei-Chung Cheng, Food and Drug Administration, Silver Spring, Maryland, USA

Abstract

A hyperspectral imaging microscope system (HIMS) was recently designed for color truth establishment of histological tissue slides used for whole slide imaging (WSI) systems color performances assessment. Here, we present the estimation procedure of the colorimetrical performance of the HIMS by measuring the transmittance spectra of spatially uniform neutral density and color filters and deriving the color coordinates in the CIELAB color space. The transmittance and CIELAB results are compared to reference transmittance spectra and subsequent CIELAB coordinates provided by measurement of the same region of interest with a spectroradiometer. To measure the same region of interest, the spectroradiometer is equipped with a fiber probe whose tip is set in one of the eyepiece tubes of the microscope. The CIE 1976 color difference, ΔE^*_{ab}, is the metric used for goodness estimation.

Introduction

Whole slide imaging (WSI) systems are color reproduction systems used in digital pathology. As medical devices, their colorimetrical performance need to be assessed since the color content of a stained pathological image has potential influence on the readers' performance and subsequent clinical diagnoses [1]. In the literature, color targets with miniature color patches were used to test WSI systems [2-4]. Such color targets were unable to represent both the spectral characteristics and microstructures of tissue samples. Recently, WSI systems were evaluated with real tissue samples based on the colorimetrical data obtained by a hyperspectral imaging microscope system (HIMS). However, the accuracy of HIMS was not reported [5].

In the present paper, we develop a test method to determine the colorimetrical performances of HIMS by analyzing the transmittance and Commission Internationale de l'Éclairage (CIE) CIELAB coordinates of spatially uniform color targets. The results are compared to measurements obtained with a reference spectroradiometer using the CIE 1976 color difference, ΔE^*_{ab}. We provide an estimation of the uncertainty on the transmittance and CIELAB coordinate results using the law of propagation of uncertainty and use Monte Carlo simulations to estimate the distribution of ΔE^*_{ab}.

Material and Methods

Experimental setup

Figure 1 presents the experimental setup. A retrofitted upright light microscope in bright field mode (AxioPhot 2, Carl Zeiss Microscopy, White Plains, NY, USA) is equipped with a tunable light source (TLS, 380 nm to 780 nm by steps of 10 nm, bandwidth 10 nm; OL490, Gooch and Housego, TX, USA) to allow the acquisition of wavelength-dependent images by a scientific monochrome charge-coupled device (CCD) camera calibrated to a linear response (Grasshopper3 9.1 MP Mono USB3 Vision, Point Grey Research Inc., BC, Canada). To improve the spatial uniformity of the HIMS illumination, the light from the tunable source is directed by a liquid guide (LG) to an integrating sphere (IS; Sphere diameter: 50.8 mm; Port Diameter: 12.7 mm; Thorlabs, Newton, NJ, USA) set before the collector lens in the illumination path. The sample is positioned on a motorized stage controlled by a Motorized Stage Controller (MSC; MAC 6000, Ludl Electronic Products Ltd., Hawthorne, NY, USA) and is imaged using a 20x objective (Plan-Apochromat 20x NA=0.8, Carl Zeiss Microscopy, White Plains, NY, USA). For comparison purposes, by measuring the same region of interest (ROI), the tip of an optical fiber connected to a reference spectroradiometer (SRM; PR-730 with fiber probe FP-730, Photo Research, Syracuse, NY, USA) is set in one of the microscope eyepiece tubes, replacing one of the regular eyepieces.

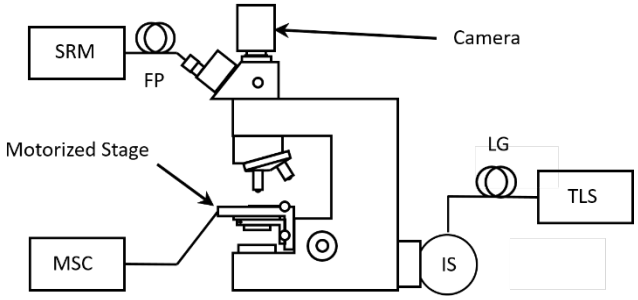

Figure 1: Schematic layout of the HIMS equipped with a PR730 spectroradiometer; SRM: spectroradiometer; FP: fiber probe; MSC: motorized stage control; IS: Integrating Sphere; LG: light guide; TLS: tunable light source

Measurements

The measurement procedure consists of measuring i) the sample in the light path and ii) no sample in the light path (100% transmittance), and for each case setting the intensity of the light engine on (regular measurement) and then off (background measurement) to account for persistent background illumination observed with the light source even when its intensity is set to zero. As an example, Figure 2 presents the light output spectrum at $\lambda = 610$ nm and shows the broadband background illumination light that remains present when the intensity parameter of the light engine is set to zero. Since the light collected by the numerical aperture of the detection fiber is naturally averaged out, 10 images are acquired at each wavelength and are spatially averaged to allow comparison to 10 measurements from the spectroradiometer. Temporal means and standard deviations over the 10 detected intensities are computed for uncertainty analysis. The transmittance values at each wavelength are then computed following

$$T(\lambda) = \frac{I_S(\lambda) - I_{SBg}(\lambda)}{I_W(\lambda) - I_{WBg}(\lambda)}, \quad (1)$$

where I_S (I_{SBg}) and I_W (I_{WBg}) are the means values of the intensities of the signal measured with the sample in the light path and with no sample in the light path, respectively, with light intensity on (off). The uncertainty on the transmittance is estimated following the law of uncertainty propagation. For a functional relationship $\boldsymbol{Y} = f(\boldsymbol{X}) = [f_1(\boldsymbol{X})f_2(\boldsymbol{X})\dots f_p(\boldsymbol{X})]$ between the output quantities $\boldsymbol{Y}$ and the input quantities $\boldsymbol{X}$, the uncertainty on $\boldsymbol{Y}$ is obtained by the Taylor expansion about $\boldsymbol{X}$ mean values, μ_X [6, 7]. The covariance matrix of $\boldsymbol{Y}$, $\boldsymbol{C_Y}$ is computed as

$$\boldsymbol{C_Y} = \boldsymbol{J}\boldsymbol{C_X}\boldsymbol{J^t}, \tag{2}$$

where $\boldsymbol{C_X}$ is the covariance matrix of $\boldsymbol{X}$ and $\boldsymbol{J}$ is the Jacobian matrix with $[J]_{ij} = \left.\frac{\partial f_i(X)}{\partial X_j}\right|_{\mu_X}$. $\boldsymbol{C_Y}$ is an approximation if $\boldsymbol{Y} = f(\boldsymbol{X})$ is non-linear. Since the measured intensities $X_i = \left(I_S(\lambda), I_W(\lambda), I_{SBg}(\lambda), I_{WBg}(\lambda)\right)$ of the sample, the 100% transmittance and backgrounds are independent, the covariance matrix is diagonal with elements $s^2_{X_i}$. The variance on the transmittance is

$$s^2_T = \sum_{i=1}^{4}\left(\frac{\partial T(\lambda)}{\partial X_i}\right)^2 s^2_{X_i}, \tag{3}$$

A first step to converting the measured transmittance to the CIELAB coordinates is to first compute the CIEXYZ tri-stimulus coordinates defined as

$$\begin{aligned} X &= K\sum_{i=1}^{N} T(\lambda_i)S(\lambda_i)\bar{x}(\lambda_i)\Delta\lambda = f_1(T) \\ Y &= K\sum_{i=1}^{N} T(\lambda_i)S(\lambda_i)\bar{y}(\lambda_i)\Delta\lambda = f_2(T), \\ Z &= K\sum_{i=1}^{N} T(\lambda_i)S(\lambda_i)\bar{z}(\lambda_i)\Delta\lambda = f_3(T) \end{aligned} \tag{4}$$

where $S(\lambda)$ is the relative spectral power of the CIE D65 standard illuminant, $\bar{x}(\lambda)$, $\bar{y}(\lambda)$ and $\bar{z}(\lambda)$ are the CIE 1931 color matching functions [8-10] and $K = \frac{100}{\sum_{i=1}^{N} S(\lambda_i)\bar{y}(\lambda_i)\Delta\lambda}$ is the normalization factor. The corresponding covariance matrix is $\boldsymbol{C_{CIEXYZ}} = \boldsymbol{J_{XYZ}}\boldsymbol{C_T}\boldsymbol{J_{XYZ}}^{\boldsymbol{t}}$ with $\boldsymbol{J_{XYZ}}$ the corresponding Jacobian. Considering N, the number of measurement wavelengths, $\boldsymbol{C_T}$ is a $N \times N$ diagonal matrix with elements $\left[{s_{T(\lambda_1)}}^2, \dots, {s_{T(\lambda_N)}}^2\right]$ defined by Eq. (3) since the transmittance measurements are independents of one another. $\boldsymbol{C_{CIEXYZ}}$ is a 3×3 covariance matrix.

The CIELAB coordinates are defined from the tri-stimulus values as

$$\begin{aligned} L^* &= 116f\left(\frac{Y}{Y_n}\right) - 16 \\ a^* &= 500\left(f\left(\frac{X}{X_n}\right) - f\left(\frac{Y}{Y_n}\right)\right), \\ b^* &= 200\left(f\left(\frac{Y}{Y_n}\right) - f\left(\frac{Z}{Z_n}\right)\right) \end{aligned} \tag{5}$$

where

$$f(t) = \begin{cases} \sqrt[3]{t} & \text{if } t > \delta^3 \\ \frac{t}{3\delta^2} + \frac{4}{29} & \text{otherwise} \end{cases} \quad with\ \delta = \frac{6}{29}, \tag{6}$$

and (X_n, Y_n, Z_n) are the tri-stimulus values for a perfectly transmitting sample. Since Eq.(6) is nonlinear, the corresponding covariance matrix is $\boldsymbol{C_{CIELAB}} \simeq \boldsymbol{J_{LAB}}\boldsymbol{C_{CIEXYZ}}\boldsymbol{J_{LAB}}^{\boldsymbol{t}}$ with $\boldsymbol{J_{LAB}}$ the corresponding Jacobian. $\boldsymbol{C_{CIELAB}}$, is 3×3 covariance matrix.

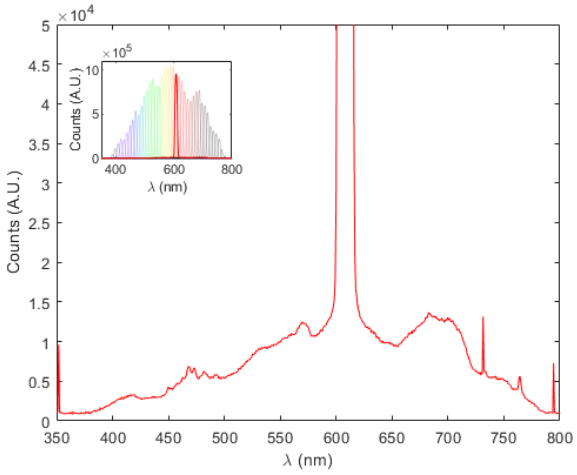

Figure 2: Spectrum output of the OL490 light engine at $\lambda = 610\,nm$. Inset: spectral output of the 41 spectral bands ($BW = 10\,nm$) used to obtain the hyperspectral images.

The metric we use to compare measurements with the hyperspectral microscope to the ground truth obtained while measuring with the spectroradiometer is the CIE 1976 color differenceΔE^*_{ab}. It is the Euclidian distance between two points with coordinates (L^*_1, a^*_1, b^*_1) and (L^*_2, a^*_2, b^*_2) in the CIELAB color space.

$$\Delta E^*_{ab} = \sqrt{\Delta L^{*2} + \Delta a^{*2} + \Delta b^{*2}}, \tag{7}$$

where $\Delta L^* = L^*_2 - L^*_1, \Delta a^* = a^*_2 - a^*_1$ and $\Delta b^* = b^*_2 - b^*_1$. Since normally distributed coordinates (L^*_1, a^*_1, b^*_1) and (L^*_2, a^*_2, b^*_2) form a distance ΔE^*_{ab} that is not normally distributed, the law of uncertainty propagation does not apply to ΔE^*_{ab}. For a given set of CIELAB coordinates (L^*_1, a^*_1, b^*_1) and (L^*_2, a^*_2, b^*_2) and their covariance

matrices obtained from the measurements with the hyperspectral microscope and the spectroradiometer, we compute their normal distribution using Monte Carlo simulations with 1000 samples. Then we compute the 10^6 ΔE^*_{ab} to obtain its statistical distribution.

Samples

We measure a set of Kodak Wratten (KW) gelatin neutral density filters ($OD = [0.1, 0.2, 0.3, 0.6, 1.0, 2.0]$) and compared the transmittance spectra acquired by the camera for linearity assessment. For colorimetrical performances assessment, we measure a set of KW color gelatin filters (#12: yellow; #25: red; #32: magenta; #47: deep blue; #58: green). For traceability assessment of the HIMS, we develop a color phantom using dots of Roscolux color filters (Figure 3). These dots are glued on a 1.4 mm-thick cardboard with a series of 24 punched holes to allow transmittance measurements. One of the punched holes is dedicated to the 100% transmittance measurements. The choice of color filters is established to match the color gamut of the hematoxylin-and-eosin (H&E) stained tissue samples to be measured by the HIMS.

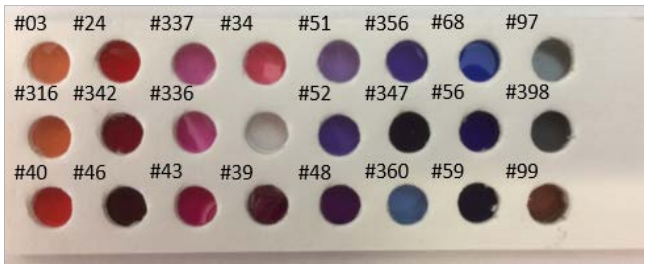

Figure 3: Color filters phantom: 23 Roscolux filters dots are glued on a cardboard slab. The empty slot is for 100% transmittance measurements.

Results

Using the set of KW gelatin neutral density filters, we compare the transmittance from the camera measurements, T_{SA}, to the transmittance from the spectroradiometer, T_S. At each wavelength, we compute a linear interpolation weighted by the uncertainty on T_{SA} and assuming T_S as the ground truth. There is a linear relationship between T_{SA} and T_S for all wavelengths in the $\lambda =$ 390 nm to 770 nm range but not for $\lambda = 380$ nm and 780 nm. At these wavelengths, the incident illumination is barely above noise level (see inset, Figure 2) which lead to huge uncertainty values on T_{SA}. One should note that at these wavelengths, the values of the color matching functions $\bar{x}(\lambda)$, $\bar{y}(\lambda)$ and $\bar{z}(\lambda)$ are small. Hence, the impact of transmittance measurements error on the CIEXYZ and CIELAB coordinates is limited. Figure 4 presents the results at $\lambda =$ 550 nm and the linear interpolation (slope $a = 1.000$, intercept $b = 1.721 \times 10^{-3}$, root mean square error rmse $= 3.880 \times 10^{-4}$). Figure 5 presents a boxplot of the distribution of ΔE^*_{ab} for the neutral density measurements.

Table 1 presents the main parameters of the statistical distribution, the 25% quartile, the median and the 75 % quartile values. For $OD =$ 0.1 to 1.0, the 75 % quartile values range from 0.53 to 1.07 when the median values range from 0.43 to 0.76. For $OD = 2.0$, the 75 % quartile is larger at 4.93 and the median value of ΔE^*_{ab} is 3.39 with upper whiskers close to 10 because of small transmittance values. There is a good agreement between the CIELAB coordinates issued from the T_S and T_{SA} measurements. However, these samples have colorimetric coordinates, i.e. a^* and b^*, close to zero and the lightness, L^*, is the only significant contributor to ΔE^*_{ab}.

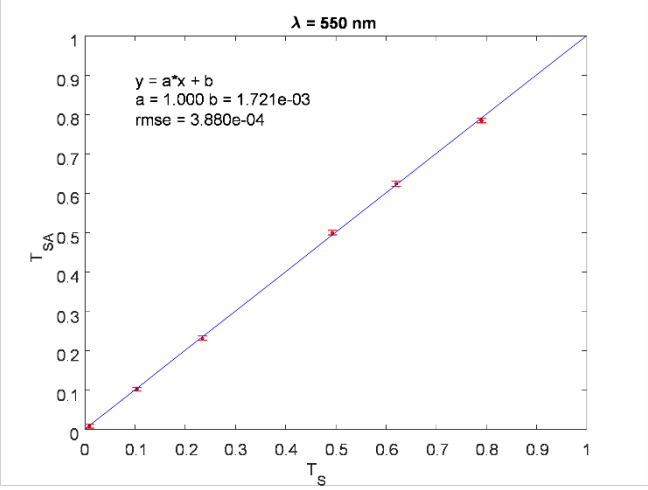

Figure 4: Comparison of the transmittance measured by the HIMS (T_{SA}) to the reference transmittance measurements by the spectroradiometer, T_S. T_{SA} versus T_S is fitted with a linear model weighted by the uncertainty on T_{SA} for $\lambda = 550\ nm$.

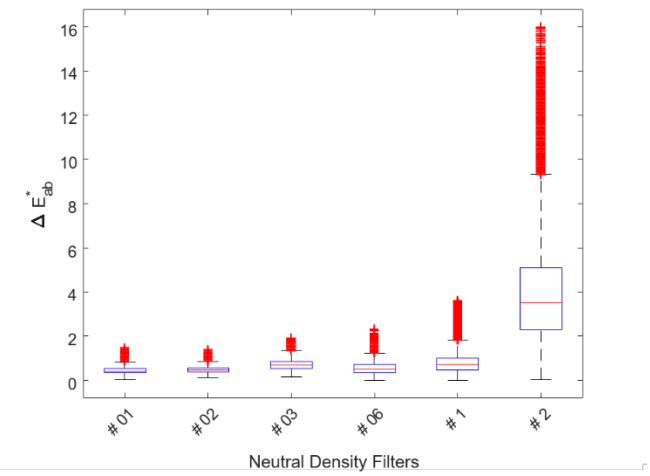

Figure 5: Boxplot of the distribution of ΔE^*_{ab} for the KW gelatin neutral density filters ($OD = [0.1, 0.2, 0.3, 0.6, 1.0, 2.0]$).

Table 1: 25% quartile, median value and 75% quartile of the ΔE^*_{ab} distribution for the KW gelatin neutral density filters ($OD = [0.1, 0.2, 0.3, 0.6, 1.0, 2.0]$)

	ΔE^*_{ab}		
	25% quartile	Median	75% quartile
OD			
0.1	0.34	0.43	0.53
0.2	0.37	0.45	0.55
0.3	0.55	0.68	0.85
0.6	0.35	0.49	0.69
1.0	0.51	0.76	1.07
2.0	2.22	3.39	4.93

For colorimetrical performances assessment of the HIMS, we first measure T_{SA} and T_S of five KW color gelatin filters. Figure 6 presents the results for filters #32 (magenta) and #47 (deep blue), two colors likely present in the color gamut of H&E stained tissues that the HIMS is designed for to measure. The agreement between T_{SA} and T_S is good within the error bars (coverage factor $k = 2$) for most wavelengths but for 380 nm, 390 nm and 780 nm where the input signal is comparable to the background signal noise level. The same behavior is true for the other color filters of the set. Figure 7 presents a boxplot of the distribution of ΔE^*_{ab} for all KW color filters whereas Table 2 sums up the significant parameters of these statistical distributions. Filters #32 and #47 have 75 % quartile values (median values) of 1.40 (1.20) and 0.94 (0.74), respectively. The red color filter #25 is also of interest for matching the H&E stain gamut but give higher values of 3.62 for the 75 % quartile and 2.13 for the median value of ΔE^*_{ab}. Filters #12 and #58 are less of a concern since they are out of the H&E color gamut. The agreement between the color coordinates issued from T_{SA} and T_S is considered reasonable.

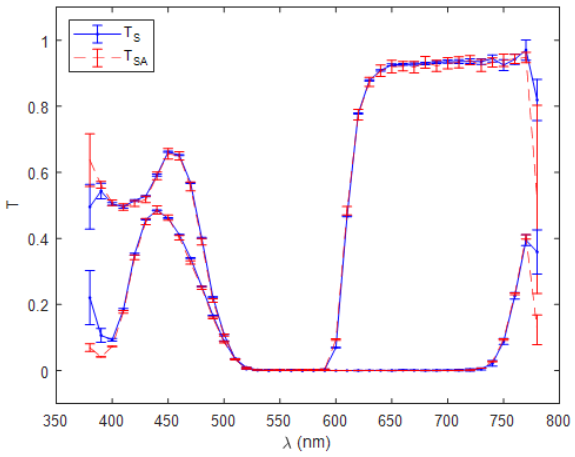

Figure 6: Transmittance spectra of KW color gelatin filters #32 (magenta) and #47 (deep blue) measured by the spectroradiometer (T_S, plain blue) and the camera (T_{SA}, dash red). T_{SA} and T_S overlap within the error bars (coverage factor $k = 2$) for $\lambda = 390$ to $770\ nm$.

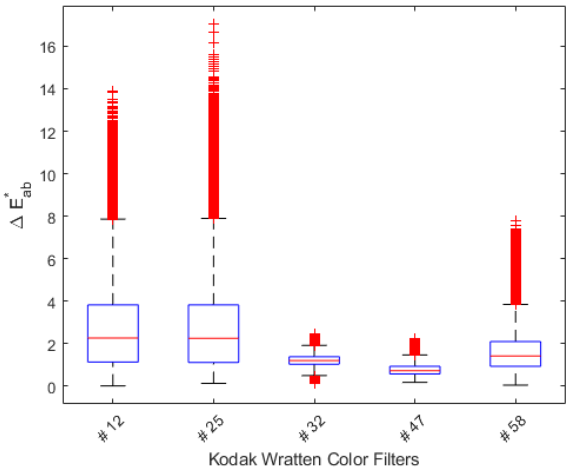

Figure 7: Boxplot of the distribution of ΔE^*_{ab} for the KW gelatin color filters (#12: yellow; #25: red; #32: magenta; #47: deep blue; #58: green)

Table 2: 25% quartile, median value and 75% quartile of the ΔE^*_{ab} distribution for the KW gelatin color filters (#12: yellow; #25: red; #32: magenta; #47: deep blue; #58: green)

	ΔE^*_{ab}		
	25% quartile	Median	75% quartile
Filter ID			
#12	1.16	2.31	3.87
#25	1.07	2.13	3.62
#32	1.01	1.20	1.40
#47	0.58	0.74	0.94
#58	0.95	1.44	2.12

Figure 8 presents the gamut of the color filters composing the traceability phantom developed by our group in the CIELAB color space along with their color appearance. Figure 9 presents a boxplot of the distribution of ΔE^*_{ab} for the phantom. The agreement between the color coordinates issued from T_{SA} and T_S is considered reasonable since the 75 % quartile values of ΔE^*_{ab} (median values) range from 0.52 to 1.59 (0.39 to 1.11). This phantom will be used

on a regular basis to check the colorimetrical performances of the HIMS.

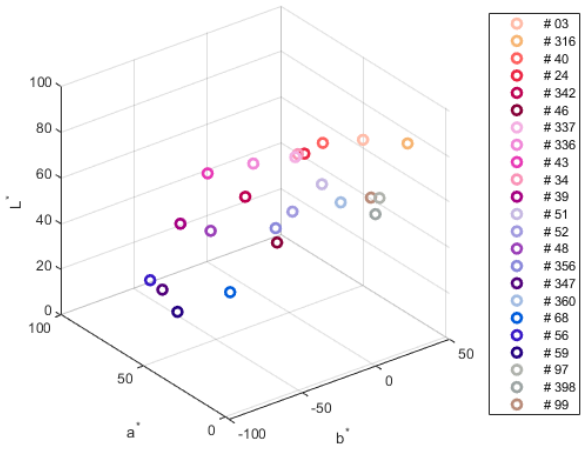

Figure 8: CIELAB coordinates of the Roscolux color filters composing the traceability phantom

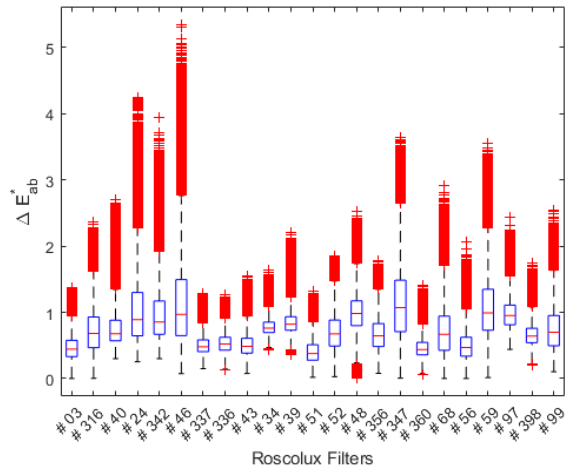

Figure 9: Boxplot of the distribution of ΔE^*_{ab} for the Roscolux filters composing the traceability phantom.

Conclusion

The HIMS can be used to establish the color truth of tissue slides used for assessing the colorimetrical performances of WSI scanners. In this study, we present the transmittance measurements and subsequent color space coordinates obtained by HIMS and compare the results to ground truth measurements established using a spectroradiometer equipped with a fiber probe whose tip is set in one of the eyepiece tubes of HIMS to measure the same ROI. We measure a set of KW neutral density filters to assess for linear relationship between transmittance measured by HIMS to the transmittance by the spectroradiometer. The results are satisfactory for $\lambda = 390$ nm to 770 nm where the tunable light source of HIMS produces an illumination that is above the background signal noise level. We assess the colorimetrical performances of HIMS first using a set of KW color filters and a traceability phantom composed of 23 Roscolux color filters. The 75 % quartile values of ΔE^*_{ab} range from 0.52 to 3.62 for filters with color in the H&E tissue stain gamut. The corresponding median values range from 0.39 to 2.13. These results are adequate for assessing commercial WSI systems, where the nominal errors are usually greater than 20 ΔE^*_{ab}.

Acknowledgments

This study was supported by the Critical Path Initiative. The authors thank Drs. Anant Agrawal, Ali Afshari, Si Wen, Aldo Badano, Ryan Beams and Andrea Kim for their technical support and comments.

Disclosure

The mention of commercial products herein is not to be construed as either an actual or implied endorsement of such products by the Department of Health and Human Services.

References

[1] E. L. Clarke, and D. Treanor, "Colour in digital pathology: a review," *Histopathology,* vol. 70, no. 2, pp. 153-163, 2017.

[2] E. L. Clarke, C. Revie, D. Brettle, M. Shires, P. Jackson, R. Cochrane, R. Wilson, C. Mello-Thoms, and D. Treanor, "Development of a novel tissue-mimicking color calibration slide for digital microscopy," *Color Research & Application,* vol. 43, no. 2, pp. 184-197, 2018.

[3] Y. Yagi, "Color standardization and optimization in whole slide imaging." p. S15.

[4] P. Shrestha, and B. Hulsken, "Color accuracy and reproducibility in whole slide imaging scanners," *Journal of Medical Imaging,* vol. 1, no. 2, pp. 027501, 2014.

[5] W. C. Cheng, F. Saleheen, and A. Badano, "Assessing color performance of whole-slide imaging scanners for digital pathology," *Color Research & Application,* vol. 44, no. 3, pp. 322-334, 2019.

[6] "Guide to the Expression of Uncertainty in Measurement (GUM)–Supplement 1: Numerical Methods for the Propagation of Distributions," *International Organization for Standardization*, 2004.

[7] B. N. Taylor, and C. E. Kuyatt, "Guidelines for evaluating and expressing the uncertainty of NIST measurement results," *NIST Technical Report 1297*, 1994.

[8] M. E. Nadal, E. A. Early, and R. R. Bousquet, "0: 45 Surface Color," *NIST Special Publication SP250-71*, 2008.

[9] "CIE S014-1/E: 2006: Colorimetry - Part I: CIE Standard Colorimetric Observer ", 2007.

[10] "CIE S014-1/E: 2006: Colorimetry - Part II: CIE Standard Illuminant ", 2007.

Author Biography

Paul Lemaillet received his PhD in physics from the University of Western Brittany (2008). For the last 15 years, he has been active in the field of bio-photonics. His specialties are in optical scattering measurements of materials and spectroscopy. He recently joined the Division of Imaging, Diagnostics, and Software Reliability (DIDSR) at the FDA to work on colorimetrical performances of imaging systems.

JOIN US AT THE NEXT EI!

IS&T International Symposium on

Electronic Imaging

SCIENCE AND TECHNOLOGY

Imaging across applications . . . Where industry and academia meet!

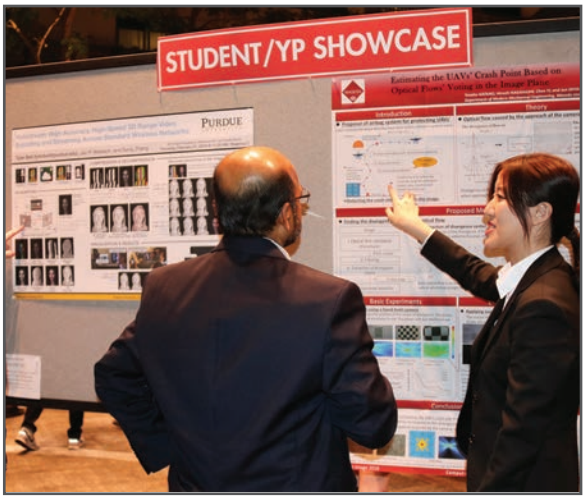

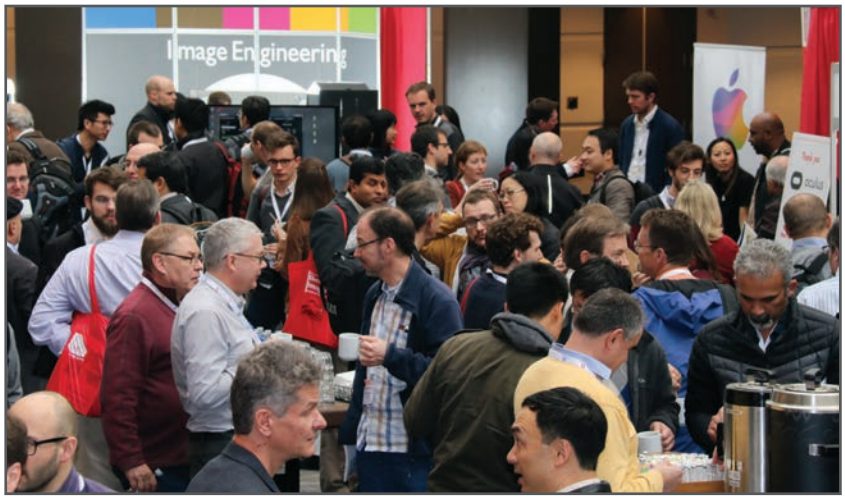

• SHORT COURSES • EXHIBITS • DEMONSTRATION SESSION • PLENARY TALKS •
• INTERACTIVE PAPER SESSION • SPECIAL EVENTS • TECHNICAL SESSIONS •

www.electronicimaging.org

IS&T
imaging.org